Structural-modulation-driven low-temperature glassy behavior in $SrRuO_3$

Chanchal Sow, D. Samal, and P. S. Anil Kumar*
Department of Physics, Indian Institute of Science, Bangalore 560012, India

A. K. Bera and S. M. Yusuf
Solid State Physics Division, Bhabha Atomic Research Centre, Mumbai 400085, India
(Received 14 May 2011; revised manuscript received 28 March 2012; published 21 June 2012)

We present a critical investigation on the structural, magnetic, and magnetotransport properties of two sets of polycrystalline $SrRuO_3$ samples with uniquely defined ferromagnetic transition temperatures. The ac magnetic susceptibility study exhibits the remarkable memory effect, a distinct characteristic of glassy behavior, at low temperatures. The transport study suggests a crossover from Fermi-liquid to non-Fermi-liquid behavior. Most strikingly, the temperature-dependent magnetoresistance exhibits two distinct dips (one around ferromagnetic ordering temperature and the other around 50 K), resembling a double-well potential in appearance. In addition, the temperature-dependent coercive field shows a plateau around 50 K. An attempt has been made to employ neutron diffraction to understand the genesis of such unusual low-temperature magnetic features. From the neutron-diffraction study, we find the evidence for changes in the unit-cell lattice parameters around 60 K and, thus, believe that the low-temperature anomalous magnetic response is closely intertwined to lattice-parameter change.

DOI: 10.1103/PhysRevB.85.224426 PACS number(s): 75.47.Lx, 75.50.Lk, 71.27.+a

I. INTRODUCTION

Now a days, one of the central themes in condensed-matter physics is to understand the strong electron-electron (el-el) correlation in solids that gives rise to a plethora of exotic new phenomena, unpredicted by conventional band theory. The correlation effect is found to be quite strong in narrow band gap "d-" or "f-" shell electron systems. In this regard, $3d/4d$ transition-metal oxide systems have continued to be an important area of research with many new discoveries viz. high-temperate superconductivity in cuprates and the colossal magnetoresistance (MR) in the manganites. Among the $4d$ transition-metal oxides, the Ru-based oxide system is more fascinating since it exhibits a rich variety of phases[1] starting from semiconducting (La_2RuO_5)[2] to metallic ferromagnet (FM) [$SrRuO_3$ (SRO)][3–5] and eventually to a p-wave triplet superconductivity in Sr_2RuO_4.[6,7] Moreover, the magnetism in the Ruddlesden-Popper series[8,9] of ruthenates $Sr_{n+1}Ru_nO_{3n+1}$ is different for different "n's." Unlike the $3d$ transition-metal oxides, $4d$ transition-metal oxides are anticipated to possess: (i) a relatively small Coulomb correlation effect (small Hubbard U) due to the large extension of $4d$ orbitals and (ii) a stronger spin-orbit interaction due to an increase in atomic number "Z." Although the evidence of large magnetocrystalline anisotropy[10–12] (MCA) in $SrRuO_3$ directly hints at stronger spin-orbit interactions, the transport and spectroscopy studies[13,14] suggest that the electron correlation effect[15] in $SrRuO_3$ cannot be ignored, and it does play an important role in determining the electronic properties of the system.[16,17] It is important to note here that the recent band-structure calculation on $SrRuO_3$ by Rondinelli *et al.*[18] estimated the on-site Hubbard term to be 0.6 eV, suggesting that the system is a moderately correlated one. Thus, one has really to take into account the electron correlation effects in ruthenates that can provide a better understanding of many of the unique phenomena.

$SrRuO_3$ is popularly known as an itinerant ferromagnet with intriguing transport and magnetic properties[19–25] and has been found to be very useful for electrodes in microelectronic devices because of its good electrical and thermal conductivities.[26,27] Moreover, it also has better chemical stability. The transport properties in metallic oxides are different from the conventional metals. The Landau-Fermi-liquid (FL) theory, which provides a firm foundation for understanding the electronic-transport properties in metals, fails in many cases of metallic oxide systems. The best example of this sort is high-T_c cuprates at optimal doping. Albeit, ruthenates form a different crystal structure[28] and exhibit absolutely different magnetic properties, but many of the anomalous responses, such as the fractional power law of electrical and optical conductivities, anomalous Raman line shapes,[23,29,30] are akin to what is observed in the normal state of high-T_c cuprates and is ascribed to non-Fermi-liquid (NFL) behavior. Besides, it is very interesting to state here that ruthenates of the same group also exhibit subtle differences in magnetic ground-state properties that strongly depend on structural distortion. For example, it is believed that $CaRuO_3$ is a quantum paramagnet[31,32] and lies on the verge of ferromagnetic instability. The different magnetic states of $SrRuO_3$ and $CaRuO_3$ are found to be due to the different structural distortions in these materials, most significantly due to the larger rotation of the octahedra in the Ca compound that significantly affects the band structure.[32,33] In essence, these materials are prone to magnetostructural coupling. Recent studies on SRO epitaxial thin films also find the same.[34]

Besides the exciting properties as described above, $SrRuO_3$ both in bulk as well as in thin-film forms, is reported to exhibit remarkable characteristics of spin-glass behavior.[10,35–37] It has to be noted here that the subject of spin glass in condensed-matter physics is one of the most complex topics and has remained at the forefront of research to understand the subtleties involved in it. Albeit, there is only a couple of

 ©2012 American Physical Society

reports which show the spin-glass-like phase in $SrRuO_3$, the microscopic understanding of the origin of such phenomena in this material is not completely understood yet. In this regard, we have undertaken an extensive study by employing various magnetic probes to understand the cryptic magnetic interaction that is responsible for the manifestation of glassy behavior in $SrRuO_3$ bulk material.

II. SAMPLE PREPARATION AND EXPERIMENTAL DETAILS

Polycrystalline samples of stoichiometric $SrRuO_3$ as well as Ru-deficient $SrRu_{(1-x)}O_3$ (with $x = 0.07$) were synthesized via the conventional solid-state reaction method using high-purity RuO_2 and $SrCO_3$ powders. In one case, we took the stoichiometric weight ratio of precursors that eventually resulted in Ru-deficient $SrRuO_3$. In the other case, we took an extra 2 wt % of RuO_2 deliberately to form stoichiometric $SrRuO_3$. After mixing the precursors according to their weight ratios, the mixed material was preheated at 900 °C for 60 h with two intermediate grindings with 100 °C/h constant heating and cooling rates. Then, it was heated again at 1100–1300 °C for about 150 h with several intermediate grindings to make a homogenous single-phase material. The powder sample was compacted into pellets and was annealed in the O_2 atmosphere at 850 °C for 12 h. All the measurements have been performed on the pellets.

The structural characterization of the sample is performed by powder x-ray diffraction (XRD) using a Bruker D8 advance x-ray diffractometer, and it is realized that both samples form a single-crystallographic phase without any impurity phases. The only distinction that we observe between the two sets of samples is with respect to Ru stoichiometry. The electron probe microanalyzer technique is employed to determine the Ru stoichiometry, and the content is found to be (0.98 ± 0.01) for one sample and is found to be 0.93 ± 0.01 for the other sample. For the sake of brevity, hereafter, we use the abbreviation SROD for the sample having relatively more Ru deficiency, and we use the abbreviation SRO for the other sample. It has to be noted here that, even after adding an extra 2 wt % of RuO_2, the Sr:Ru is within an inch of stoichiometry but not exactly at 1:1. This is probably due to the conspicuous volatility of RuO_2 at elevated temperatures. The scanning electron microscopy studies revealed an average particle size of ~ 4 μm for both samples. The dc magnetization measurements are performed in the temperature range of 10–300 K and a magnetic field up to 5 T using a Quantum Design superconducting quantum-interference device magnetometer. Ac susceptibility measurements are carried out by a commercial CryoBIND system down to a temperature of 4.2 K and in the frequency range of 15 Hz to 1 KHz. The magnetotransport properties are measured using the standard four-probe van der Pauw configuration with the magnetic field (up to 11 T) applied perpendicular to the current direction. Silver indium contacts were used to give four-probe connections to both samples. The temperature-dependent (5–200-K) neutron-diffraction (ND) study is carried out using the Dhruva reactor, Trombay (India), and the structural as well as the magnetic information has been extracted out of that.

III. RESULTS AND DISCUSSION

A. Structural analysis

Figures 1(a) and 1(b) show the typical Rietveld-refinement x-ray diffraction patterns for both sets of samples. The refinement has been carried out using the general structure analysis system (GSAS) code.[38] It is found that there is good agreement between observed and calculated profiles. Both of the samples crystallize in the orthorhombic crystal structure (*Pnma* space group), and the lattice parameters are tabulated in Table I. The refined structural parameters agreed well with those reported in the literature.[39]

B. Magnetization

Figures 2(a) and 2(b) show the temperature-dependent magnetization [field cooled (FC) and zero-field cooled (ZFC)] measured at 100 Oe for SRO and SROD, respectively. The FC curve shows Brillouin-function-like behavior, which is a typical characteristic of a ferromagnet. The ZFC curve shows a peak around 162 and 150 K, corresponding to FM ordering temperatures, for SRO and SROD, respectively. From Figs. 2(a) and 2(b), it is evident that the FC and ZFC curves bifurcate from each other largely in the ferromagnetic phase. The reason for such large splitting between FC and ZFC curves directly indicates the existence of huge MCA present in the system. In general, the magnetic anisotropy hinders the rotation of the moment toward the direction of the applied field, and hence, the more the MCA is, the larger the splitting is. Our finding of large FC-ZFC splitting supports the results of

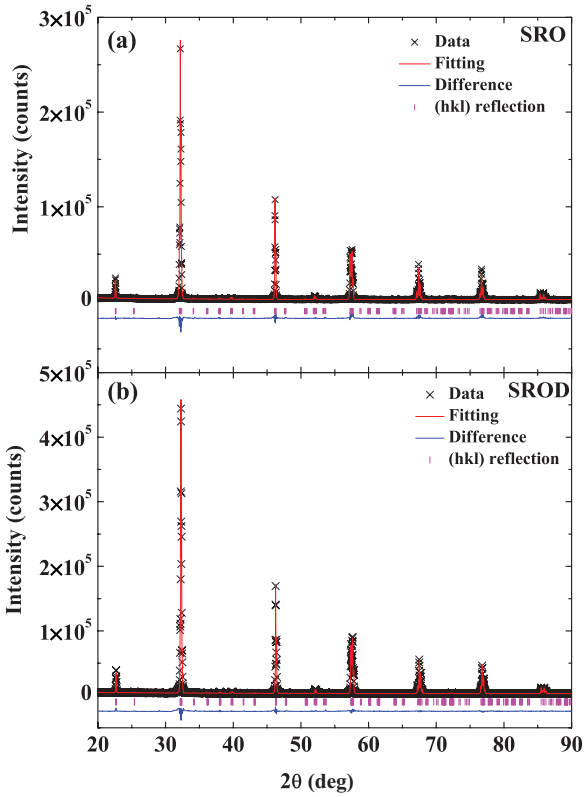

FIG. 1. (Color online) Rietveld-refined profiles for (a) SRO and (b) SROD.

TABLE I. Refined lattice constants and different agreement factors obtained from the x-ray diffraction study.

Sample	Space group	a (Å)	b (Å)	c (Å)	χ^2	R_P	R_{WP}
SRO	*Pnma*	5.5709(1)	7.8461(1)	5.5311(1)	2.94	0.065	0.087
SROD	*Pnma*	5.5652(1)	7.8439(1)	5.5303(1)	3.23	0.047	0.056

an earlier paper by Kanbayasi,[11] on the single crystal of SRO, where he observed a large amount of cubic MCA with an easy axis of magnetization along the [100] or [010] direction. Moreover, a careful inspection of the ZFC curve reveals a broad hump for both of the samples below 70 K. Besides, we also observe a change in the trend of the dM/dT vs the T plot for the FC curve around the same temperature. Thus, the low-temperature unusual feature, observed both in the FC and ZFC curves, indicates that there exists a feeble hidden magnetic interaction in addition to the strong FM interaction. The spontaneous magnetization below T_c follows the scaling law $M \sim (T_c - T)^{\beta}$ with $\beta = 0.300 \pm 0.004$ and 0.350 ± 0.008 for SRO and SROD, respectively. This indicates a three-dimensional (3D) Ising-type ferromagnetic behavior since the theoretical value of β, obtained from the 3D Ising model, is approximately 0.32.[40] However, it is worth mentioning here that the value of the critical exponent for this system continues to be a topic of controversial debate in the literature. The early paper by Kats *et al.*,[41] on the $SrRuO_3$ thin film, obtained the exponent to be 0.325 and interpreted it on the basis of Ising behavior. However, the later paper by Kim *et al.*,[42] on a single crystal of $SrRuO_3$, obtained it to be 0.5 and interpreted it on the basis of mean-field behavior. The paper by Wang *et al.*,[43] on SRO films grown on $SrTiO_3$ (STO), further obtained the values of 0.43 and 0.34 for [110] and [010] orientations, respectively, and suggested that the critical exponent seems to be dependent on the magnetization orientation. However, the recent paper by Palai *et al.*,[10] on SRO films grown on STO, obtained the value to be 0.369 and 0.313 for [110] and [010] orientations, respectively, and believed that the different values could be related to different domain structures, orientation, or strain effect associated with two different crystallographic-oriented films.

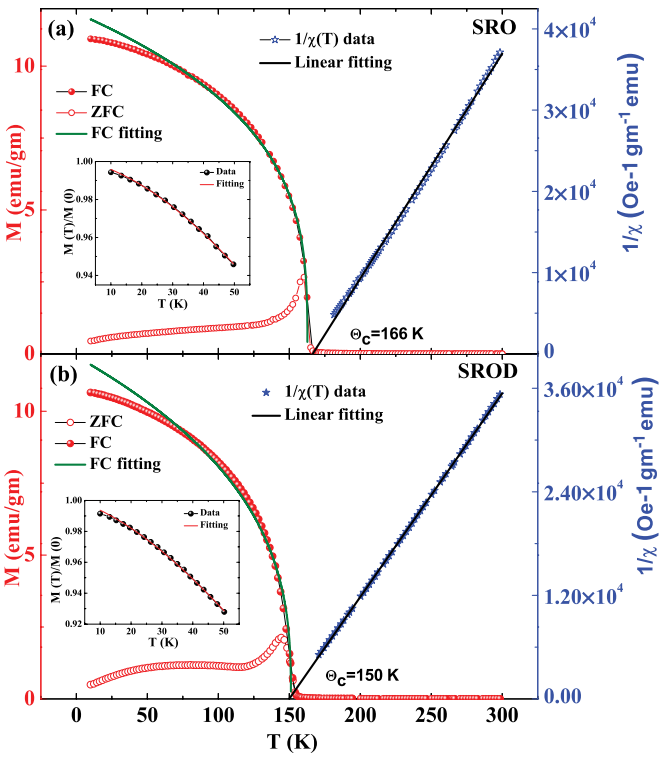

FIG. 2. (Color online) (Left) Temperature dependence of FC and ZFC dc magnetization for (a) SRO and (b) SROD measured at 100 Oe. The solid lines are the fitted curves according to $M \sim (T_c - T)^{\beta}$. (Right) The temperature dependence of reciprocal susceptibility for (a) SRO and (b) SROD. Solid lines show the Curie-Weiss linear fit. The insets in both (a) and (b) show the $M(H,T)/M(H,0)$ vs the T plot. The solid line shows the fitting according to the equation $M(H,T) = M(H,0)[1 - A_{SW}T^{3/2} - B_{SE}T^{2}]$.

Furthermore, we have looked at the low-temperature thermal evolution of magnetization for both sets of samples. It is worth mentioning here that, in the case of an itinerant ferromagnet, the low-temperature magnetization usually gets reduced with the increase in temperature both by thermally excited magnons as well as Stoner excitations. However, unlike the Bloch $T^{3/2}$ law for magnons, the Stoner excitation follows T^2 dependence. Based on this approximation, the low-temperature FC magnetization data are fitted to $M(T)/M(0) = 1 - A_{SW}T^{3/2} - B_{SE}T^2$, where $M(0)$ is the magnetization at 0 K, A_{SW} is the spin-wave parameter, and B_{SE} is the Stoner excitation parameter. $M(0)$ is obtained by extrapolating the field cooled $M(T)$ to $T = 0$ K, and its values are found to be 11.089 and 10.814 emu/gm for SRO and SROD, respectively. The insets in Figs. 2(a) and 2(b) show the fitting of low-temperature magnetization data to $M(T)/M(0) = 1 - A_{SW}T^{3/2} - B_{SE}T^2$. From this fit, the parameter A_{SW}, B_{SE} is found to be $1.15 \times 10^{-4}T^{-3/2}$, $5.38 \times 10^{-6}T^{-2}$ and $2.03 \times 10^{-4}T^{-3/2}$, $4.31 \times 10^{-7}T^{-2}$ for SRO and SROD, respectively. It is found that, even in the absence of the T^2 correction, the data fit reasonably well with the Bloch $T^{3/2}$ law, indicating a weaker Stoner excitation cross section. The A_{SW} parameter, thus, obtained is marginally different in this case. Using the spin-wave parameter, it is possible to calculate the exchange interaction (J) between two Ru^{+4} atoms since J is proportional to $A_{SW}^{-2/3}$. In particular, $A_{SW} = (0.0587S)(2k_BJS)$, where $S = 1$ is the total spin of Ru^{+4} ($t_{2g}^4 e_g^0$) and k_B is the Boltzmann constant.[31] Setting all the values of known parameters, J is found to be $31.78k_B$ and $22.23k_B$ for SRO and SROD, respectively. The larger J obtained for SRO clearly explains why it has a higher Curie temperature than SROD. Moreover, it is worth mentioning here that the value of J as well as T_c obtained for the SROD sample very closely match the values reported for epitaxial thin films.[10]

Figure 3(a) shows the M-H plot at 2 K for SRO and SROD samples. Magnetization tends to increase sharply toward saturation with the increase in applied field. However, a careful

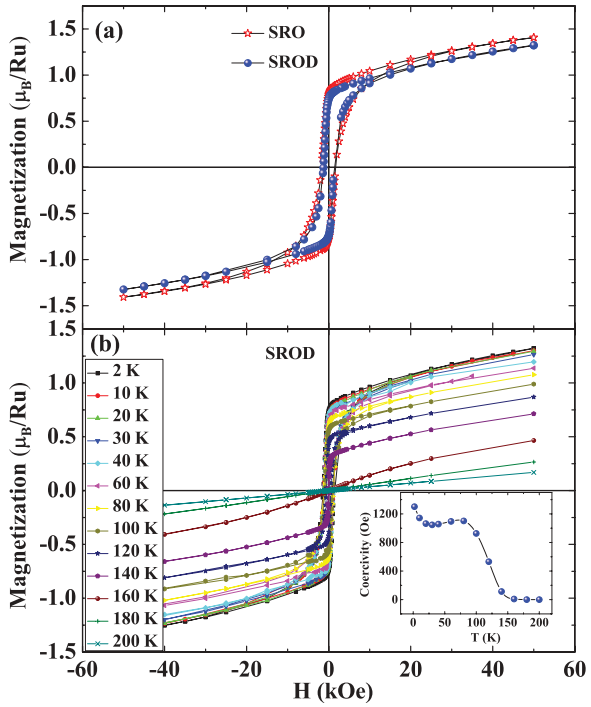

FIG. 3. (Color online) (a) M-H loops for the SRO and SROD samples at 2 K and (b) shows the same at various temperatures for the SROD sample. The inset in (b) displays coercivity vs temperature.

inspection finds that a small nonsaturating component appears to be superimposed on the saturating FM component and, thus, prevents the magnetization from being in a fully saturated state even at larger applied magnetic fields. Our estimation for the saturation value of the magnetization from the M-H plots at 2 K is found to be 1.41 and 1.32 μ_B/Ru for SRO and SROD, respectively. These moments are much smaller than the expected spin-only moment of 2.0 μ_B ($\mu = gS\mu_B$, where $S = 1$ for Ru) for $SrRuO_3$ based on the ionic model. Some of the earlier reports on $SrRuO_3$ find that, even after applying a field of 30 T, the saturation moment hardly reaches 1.5 μ_B/Ru.[33] So, it has become a fundamental concern to understand the lack of saturation moment in $SrRuO_3$. The plausible reasons that one can think of for such effects are as follows: (a) There might be some kind of hidden antiferromagnetic (AF) interaction existing in the ferromagnetic domain; (b) since it is an itinerant ferromagnetic system, the total moment is expected to be less compared to the calculated moments based on the ionic model; (c) it might have a complex spin configuration, such as spin canting at the surface that can result in a reduced saturation moment; and (d) the slow growth of domains might lead to an incomplete alignment of the magnetization.

Figure 3(b) shows the M-H plot at various temperatures starting from 2 to 200 K for the SROD sample. In the inset of Fig. 3(b), we show the coercivity (H_c) vs the temperature plot for SROD. Generally, for a ferromagnet, H_c increases as we decrease the temperature. But, from the inset in Fig. 3(b), it is astonishing to note that H_c exhibits an unusual behavior toward low temperatures. The unexpected behavior in the H_c vs the T plot is intriguing, and it is hard to understand from the conventional ferromagnetic description. However, we envisage that it might be directly connected to the broad hump observed in the ZFC curve.

C. Relaxation and memory

Figure 4(a) displays the normalized in-phase ac susceptibility component $\chi'(T)$ measured at a frequency of $f = 420$ Hz and in an applied $H_{ac} = 0.17$ Oe. It is observed that the sample exhibits a broad hump around 70 and 50 K in addition to a sharp peak at 162 and150 K for SRO and SROD, respectively. The sharp peak position is frequency independent and corresponds to the FM ordering temperature. But on the other hand, the position of the low-temperature hump is frequency dependent and is clearly shown in Figs. 4(b) and 4(c). However, it is bewildering to note here that, as we increase the frequency, the hump position shifts toward the lower temperature, and it is very much unlike what is usually observed for a canonical spin-glass system. It has to be mentioned here that, in the case of the $NaNiO_2$ antiferromagnet, a similar trend has been noticed and has been explained on the basis of multiple relaxation rates.[44] To have a further understanding, we have carried out the experiment related to memory effect.[45–48] Generally, time-dependent phenomena, such as aging, memory, etc., arise in disordered glassy systems. The state of such systems is described by the multivalley metastable energy landscape that

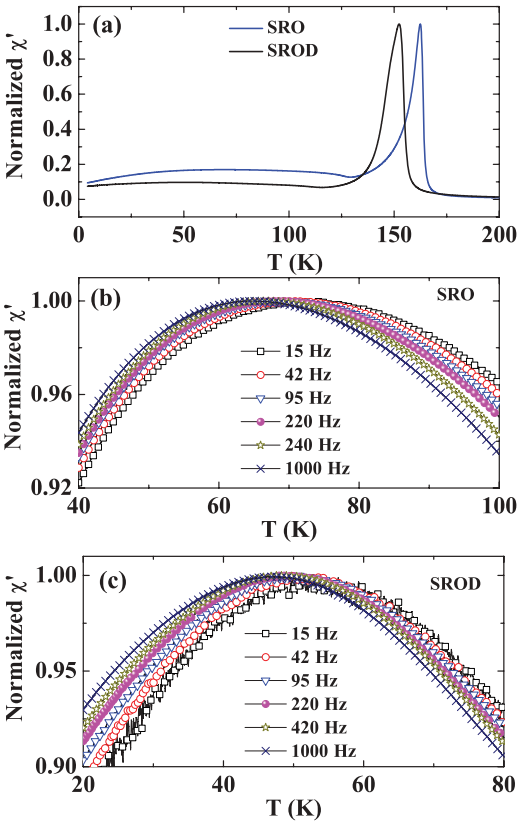

FIG. 4. (Color online) (a) Temperature dependence of the in-phase component of ac susceptibility for SRO and SROD samples measured at $f = 420$ Hz; (b) and (c) show the zoomed-in view of the temperature dependence of the normalized in-phase ac susceptibility component measured at various frequencies for SRO and SROD, respectively.

exhibits slow dynamics. Due to the inherent slow dynamics associated with the glassy system, it does not reach the equilibrium state within the experimental time scale. As a result, this leads to time-dependent generic nonequilibrium phenomena. The memory effect can clearly be elucidated by measuring χ_{ac} in two different ways, namely, (i) the halting mode of measurement (χ_{halt}) and (ii) the reference mode of measurement (χ_{ref}). In the halting mode of measurement, the sample is first zero-field cooled from room temperature to the lowest temperature with an intermediate halt (t_{halt}) for about ~12 h at the halting temperature (T_{halt}). Then, the magnetic response (χ_{halt}) is recorded during the heating run by applying a probing ac field (H_{ac}). However, in the reference mode of measurement, the sample is zero-field cooled from room temperature to the lowest possible temperature without any intermediate halt, and then regular ZFC data (χ_{ref}) are recorded during the heating run with the same H_{ac}. To demonstrate the memory effect more efficiently, we plot $\Delta\chi' = (\chi'_{ref} - \chi'_{halt})$ vs T, and the observed peak in $\Delta\chi'$ around the T_{halt} reflects the memory effect, indicating glassiness present in the material. Figure 5 shows the $\Delta\chi' = (\chi'_{ref} - \chi'_{halt})$ vs the T plot for SROD at various halting temperatures (20, 40, and 100 K). We also observe a peak in $\Delta\chi'$ at $T_{halt} = 30$ K for SRO, which is shown as the inset in Fig. 5. From Fig. 5, it is evident that both sets of samples exhibit peaks in $\Delta\chi'$ around the corresponding T_{halt}, except at 100 K, which is well above the temperature corresponding to the hump positions. In fact, the remarkable observation of the memory effect in bulk SRO illustrating the glassy behavior. We believe that the manifestation of low-temperature glassy behavior and a hump in the χ' vs T data has a common origin. The observation of glassy phenomena in the case of itinerant ferromagnetic systems, such as $SrRuO_3$, is unconventional and needs meticulous studies to understand the underlying physics behind it. However, at this point in time, we think of the following two possible reasons that can be attributed to the manifestation of such an effect. In an ideal ferromagnet, domain growth involves microscopic time scales. However, in the real world, no ferromagnet is completely devoid of disorder or defects. In the presence of such a pinning disorder, there can be a multitude of metastable states that allows the domain walls to have thermally activated hopping from one state to another. This process does not allow the system to reach the equilibrium state within the experimental time scale and, hence, can lead to nonequilibrium phenomena, such as memory and aging effects.[49,50] It is also quite possible that the system can show such effects if spin canting happens to occur either in the bulk or on the surface of the sample.[51] The spin canting can produce finite spin clusters that essentially consist of sets of noncollinear ferromagnetically or antiferromagnetically coupled spins embedded in the $SrRuO_3$ ferromagnetic matrix. In essence, if the spin canting could render disorder and frustration (two key ingredients required for the occurrence of spin-glass phenomena), then the system will tend to exhibit such glassy phenomena. As described earlier, the lack of saturation magnetic moment inferred from the M-H plot, indeed, indicates the possible existence of spin canting or antiferromagnetically coupled spins in a ferromagnetic matrix.

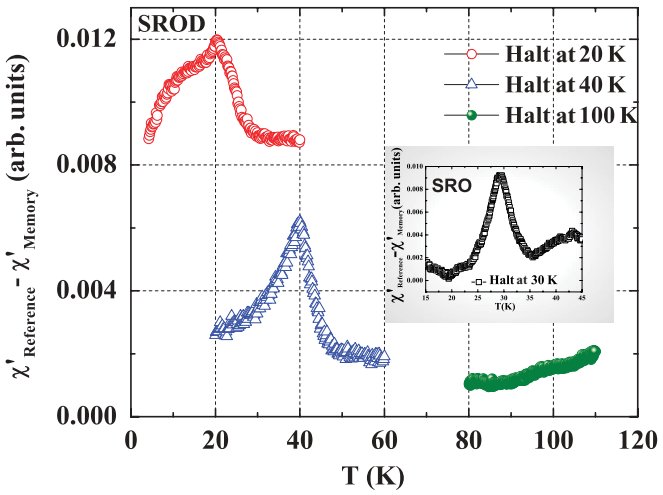

FIG. 5. (Color online) The differential in-phase ac susceptibility $\Delta\chi' = (\chi'_{ref} - \chi'_{halt})$ vs the T plot at various halting temperatures ($T_{halt} = 20$, 40, and 100 K) for SROD. The inset shows the same plot for SRO at $T_{halt} = 30$ K.

D. Transport

Figures 6(a) and 6(b) show the temperature-dependent resistivity in the zero and applied fields of 11 T for both sets of samples. The zero-field resistance vs the temperature curve shows metallic behavior and exhibits a change in slope around 160 and 150 K, corresponding to a transition from a paramagnetic state to a ferromagnetic state for SRO and SROD, respectively. A careful inspection finds a low-temperature upturn in resistivity for SROD, and it is clearly shown as the lower inset in Fig. 6(b). This indicates the occurrence of a metal-insulator-like transition that possibly could arise due to the disorder-induced localization effect.[52–54]

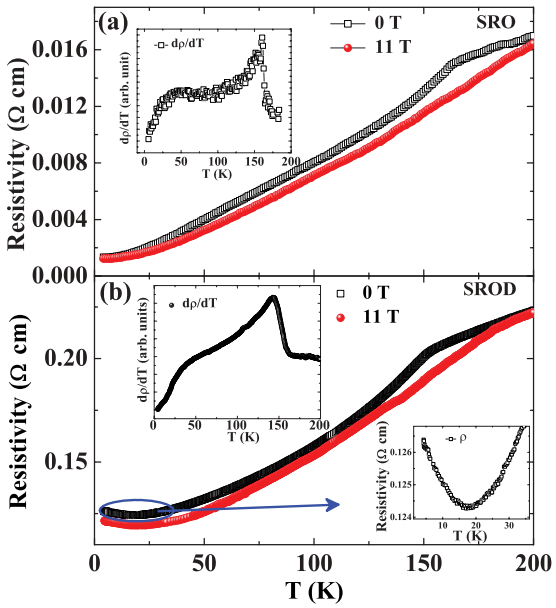

FIG. 6. (Color online) The temperature-dependent resistance for (a) SRO and (b) SROD in $H = 0$ and 11 T. The upper insets in (a) and (b) show the $d\rho/dT$ vs the T curve for $H = 0$ T. The lower inset in (b) shows the zoomed-in view of the ρ vs the T plot in the zero field for SROD.

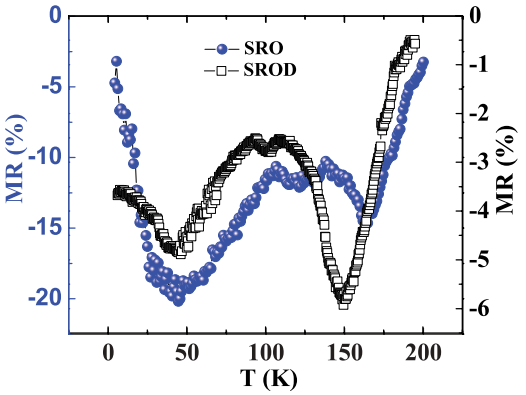

FIG. 7. (Color online) MR as a function of temperature for both sets of samples.

It is well known that the magnetic and the transport behaviors of $SrRuO_3$ are very sensitive to Ru content, Ru-O-Ru distance, and bond angle. Since SROD is Ru deficient, there could be rupture of the conduction path within the RuO_6 octahedron due to vacant Ru sites, and this might lead to metal-insulator transitionlike phenomena.

We have extensively studied the MR behavior of both sets of samples up to a field of 11 T. The MR is defined as $[R(H) - R(0)]/R(0)$, where $R(H)$ and $R(0)$ correspond to the resistance in the presence of a magnetic field and a zero field, respectively. It is found that the MR vs the T plot (Fig. 7) exhibits two distinct negative maxima for both samples, one around 50 K and the other in the vicinity of T_c. Generally, for ferromagnetic metallic oxide systems, a maximum in MR is expected to occur around the Curie temperature owing to large spin fluctuation, and as the temperature decreases, the system gradually improves its magnetic order, and the MR decreases. However, the observation of maximum in MR around ~50 K is mysterious and conspicuously indicates the emergence of a hidden magnetic ordering at low temperatures. This further reinforces, if one carefully notices, the behavior of the $d\rho/dT$ vs the T curve, shown as the upper insets in Figs. 6(a) and 6(b). It is evident that the $d\rho/dT$ vs the T curve shows a change in slope around 50 K. Thus, we realized that the unusual low-temperature magnetic behavior, as evidenced from ZFC dc magnetization and ac susceptibility studies, has a direct influence on the transport properties. In essence, the magnetic and transport properties in $SrRuO_3$ are found to be strongly correlated.

Furthermore, a careful investigation on the temperature-dependent transport data reveals a crossover from FL behavior to NFL behavior around 40 K. Based on Landau's phenomenological FL theory for metals, the el-el scattering cross section varies quadratically (T^2) with temperature. In Fig. 8(a), we show the low temperature ρ vs the T plot that fits reasonably well to T^2 dependence, i.e., $\rho = \rho_{0A} + AT^2$ up to a temperature of 40 K. The values of the fitting parameters are found to be $\rho_{0A} = 1.3 \times 10^{-2}$ Ω cm and $A = 1.27 \times 10^{-6}$ Ω cm K^{-2} for SRO. Furthermore, it is known that the electron-magnon-scattering cross section also follows T^2 dependence, akin to the el-el scattering. So, it is really hard to separate out the individual contribution from the low temperature ρ vs the T plot. However, a qualitative statement

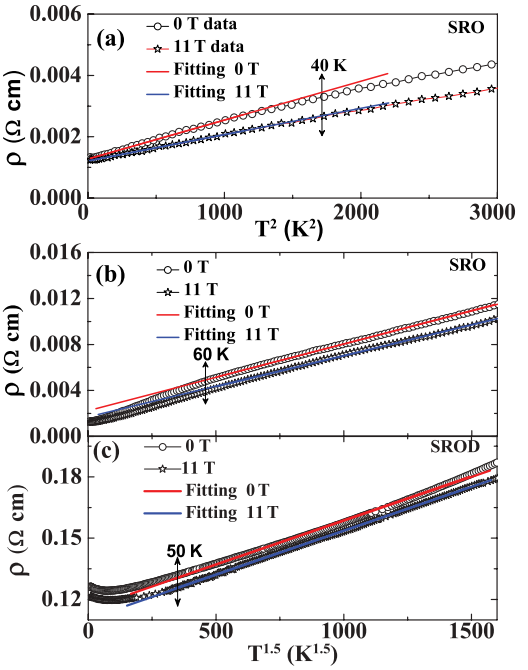

FIG. 8. (Color online) (a) The ρ vs the T^2 plot over the temperature range of 4.2–200 K for SRO in $H = 0$ and 11 T. Solid lines are linear fits to the data according to $\rho = \rho_{0A} + AT^2$ over the temperature range from 4.2 to 40 K in $H = 0$ and 11T; (b) and (c) show the ρ vs the $T^{1.5}$ plot in $H = 0$ and 11 T for SRO and SROD, respectively. Solid lines are linear fits to the data according to $\rho = \rho_{0B} + BT^{1.5}$ over the temperature range from 4.2 to 40 K in $H = 0$ and 11 T.

can be made about the contribution of the electron-magnon scattering to resistivity by inspecting the values of the fitting parameters at zero fields and in the presence of an applied magnetic field. In the presence of an applied magnetic field, the coupling between electrons and magnons produces significant spin-flip scattering, and therefore, the coefficient A is expected to be field dependent. Since we notice, from our fitting, that the coefficient A in the zero field and in the presence of the field (11 T) is almost identical, we believe that electron-magnon scattering has a negligible contribution to resistivity. Moreover, it is observed that, as the temperature increases above 40 K, the ρ vs the T plot does not follow T^2 dependence. Rather, it follows $T^{1.5}$ dependence in the temperature range from 60 to 140 K, signifying the NFL-like behavior. Figures 8(b) and 8(c)

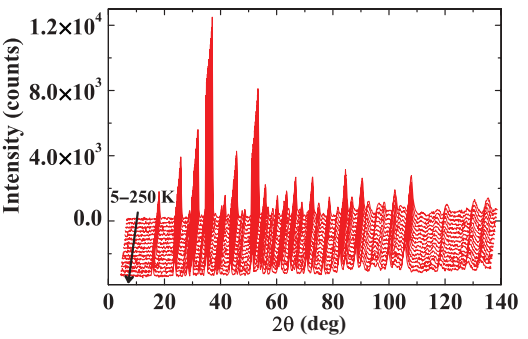

FIG. 9. (Color online) Neutron-diffraction pattern at various temperatures (5–250 K) for SRO.

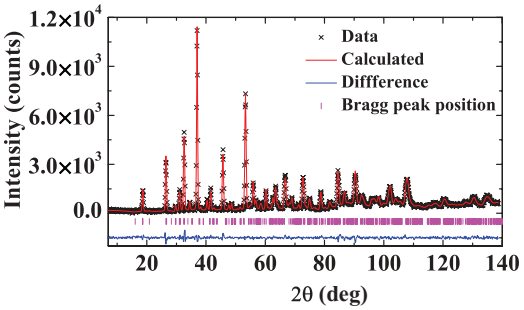

FIG. 10. (Color online) Rietveld-refined profile of the neutron-diffraction pattern at 250 K for SRO.

illustrate the $T^{1.5}$ dependence of ρ for both sets of samples. Although the underlying mechanistic understanding for the observation of NFL-like behavior in $SrRuO_3$ is being debated, it is strongly attributed to the spin fluctuations. It is remarkable to note here that all the anomalous behaviors discussed so far are prominent below 60 K, the temperature at which the transport data deviate from the NFL behavior.

E. Neutron diffraction

In order to have further insight into the origin of the puzzling low-temperature magnetic behavior of $SrRuO_3$, we have undertaken a systematic temperature-dependent neutron-diffraction study in the range of 5–250 K. Figure 9 shows various ND patterns for the SRO sample recorded at different temperatures over 5–250 K. With the lowering of temperature, we only observe an increase in the intensity of the fundamental Bragg peaks at the lower angular range below ∼160 K. This confirms the ferromagnetic ordering but no structural phase transition below ∼160 K. Figure 10 shows the Rietveld-refined ND pattern for SRO at 250 K. In agreement with the x-ray diffraction study and previous reports,[55] the Rietveld analysis also confirms an orthorhombic crystal structure with space group *Pnma*. The refined lattice parameters are in good agreement with the same parameters obtained from the x-ray diffraction study. A comparison of the lattice parameters obtained from the XRD and ND studies is given in Table II.

Figure 11(a) shows the temperature dependence of lattice parameters obtained from the Rietveld analysis of the ND patterns. For completeness, we also note the values of lattice parameters and the unit-cell volume for all measured temperatures for SRO in Table III. From Fig. 11(a), it is evident that the lattice parameters undergo a gradual change around the ferromagnetic transition temperature. It is noticed that the *c*-axis lattice parameter shows a compression as we move from the high-temperature paramagnetic phase to the low-temperature ferromagnetic phase. On the contrary, the lattice parameters for the "*a*" and "*b*" axes show an expansion.

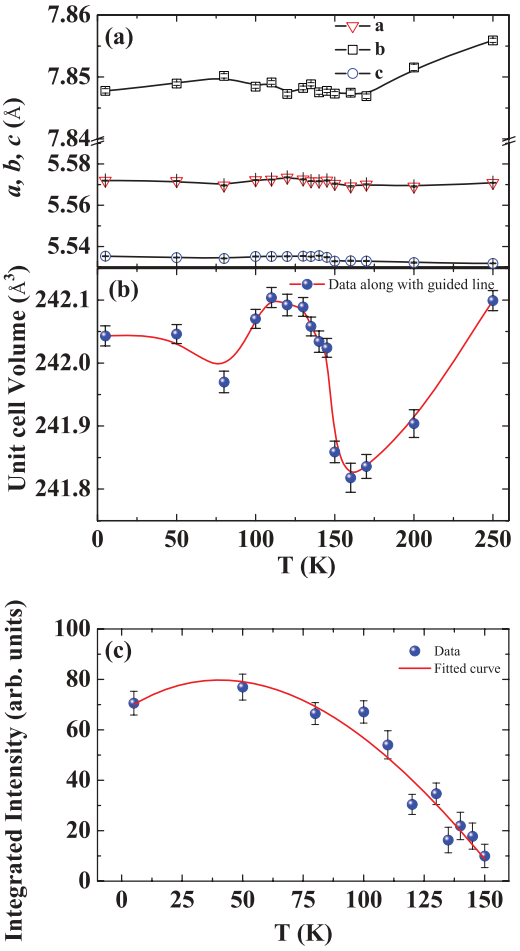

FIG. 11. (Color online) (a) and (b) represent the modulation in the lattice parameters and the unit-cell volume, respectively, over the temperature range of 5–250 K and (c) integrated magnetic intensity of the (101) and (020) Bragg peaks vs temperature.

For better realization, we show the changes in the unit-cell volume as a function of temperature in Fig. 11(b). From Fig. 11(b), it is unequivocal that the unit-cell volume shows an unusual modulating behavior as a function of temperature, and more surprisingly, we observe two troughs, the prominent one around the ferromagnetic ordering temperature and the other at a lower temperature (∼75 K). This clearly signifies the change in unit-cell parameters around the corresponding temperatures. Also, we observe a decrease in the integrated magnetic intensity [shown in Fig. 11(c)] below ∼50 K. For a final remark about RuO_6 octahedral tilting as usually noticed in ruthenates, we have analyzed the temperature-dependent ND data at great lengths. Our analysis finds that the octahedral tilting has a fairly large amount of tilting (of about 8° to 9°) with respect to the *b* axis.

TABLE II. The 250-K ND Rietveld-refinement results in comparison with the room-temperature XRD results.

Expt.	Space group	*a* (Å)	*b* (Å)	*c* (Å)	χ^2 (%)	R_P	R_{WP}
ND (SRO)	*Pnma*	5.5691(3)	7.8452(5)	5.5271(3)	4.64	0.058	0.079
XRD (SRO)	*Pnma*	5.5709(1)	7.8461(1)	5.5311(1)	2.94	0.065	0.087

TABLE III. The refined values of lattice constants a, b, and c as well as the unit-cell volume obtained from the ND pattern at all measured temperatures over 5–250 K.

T (K)	a (Å)	Error in a (Å)	b (Å)	Error in b (Å)	c (Å)	Error in c (Å)	V (Å^3)	Error in V (Å^3)
5	5.571 91	2.10×10^{-4}	7.847 76	3.40×10^{-4}	5.535 32	2.00×10^{-4}	242.043	0.016
50	5.571 74	2.10×10^{-4}	7.848 94	2.80×10^{-4}	5.534 71	1.90×10^{-4}	242.046	0.015
80	5.5696	2.30×10^{-4}	7.850 17	3.50×10^{-4}	5.534 26	2.00×10^{-4}	241.97	0.017
100	5.572 19	2.10×10^{-4}	7.848 44	2.80×10^{-4}	5.535 18	1.90×10^{-4}	242.07	0.015
110	5.572 45	2.20×10^{-4}	7.849 12	3.00×10^{-4}	5.535 23	1.90×10^{-4}	242.104	0.016
120	5.573 48	2.40×10^{-4}	7.847 25	3.10×10^{-4}	5.535 24	2.10×10^{-4}	242.092	0.017
130	5.572 52	2.10×10^{-4}	7.848 24	2.90×10^{-4}	5.535 42	1.90×10^{-4}	242.089	0.015
135	5.571 66	2.00×10^{-4}	7.848 83	2.70×10^{-4}	5.535 16	1.80×10^{-4}	242.058	0.015
140	5.5716	2.30×10^{-4}	7.847 52	3.20×10^{-4}	5.535 58	2.10×10^{-4}	242.034	0.017
145	5.571 99	2.10×10^{-4}	7.847 76	2.60×10^{-4}	5.534 80	2.00×10^{-4}	242.024	0.015
150	5.570 43	2.30×10^{-4}	7.847 31	3.30×10^{-4}	5.532 89	2.10×10^{-4}	241.859	0.017
160	5.569 18	3.00×10^{-4}	7.847 47	4.50×10^{-4}	5.533 10	2.90×10^{-4}	241.818	0.023
170	5.570 09	2.50×10^{-4}	7.8469	3.70×10^{-4}	5.533 00	2.50×10^{-4}	241.836	0.019
200	5.569 13	2.60×10^{-4}	7.851 55	5.10×10^{-4}	5.532 23	2.60×10^{-4}	241.904	0.022
250	5.570 89	2.00×10^{-4}	7.855 91	3.40×10^{-4}	5.531 87	2.00×10^{-4}	242.099	0.016

IV. THE EFFECT OF Ru DEFICIENCY

For gaining a better insight into such anomalous low-temperature glassy behavior against the sample composition with respect to Ru content, we have undertaken an elaborate study on three more sets of samples by deliberately varying the Sr/Ru ratio. The stoichiometry of these three sets of samples is found to be $SrRu_{0.94\pm0.01}O_3$, $SrRu_{0.96\pm0.01}O_3$, and $SrRu_{0.99\pm0.01}O_3$. We have performed a detailed ac susceptibility study, and it is found that the ferromagnetic transition temperature varies with the Ru deficiency systematically as shown in Fig. 12. This observation is in good agreement with the one by Dabrowski *et al.*,[56] who noticed a decline in the ferromagnetic transition temperature with an increase in Ru-site vacancy. Concerning the possible existence of glassy behavior in the above nonstoichiometric samples, we have performed the memory experiment using the same protocol as described earlier. Figure 13(a) shows the $\Delta\chi' = (\chi'_{\rm ref} - \chi'_{\rm halt})$ vs the T plot for $SrRu_{0.99\pm0.01}O_3$ at the halting temperature of 40 K with three different halting times of 2, 4, and 8 h. It is interesting to note that, even with a halting time of only 2 h, we see a clear peak, indicating the signature of the memory effect.

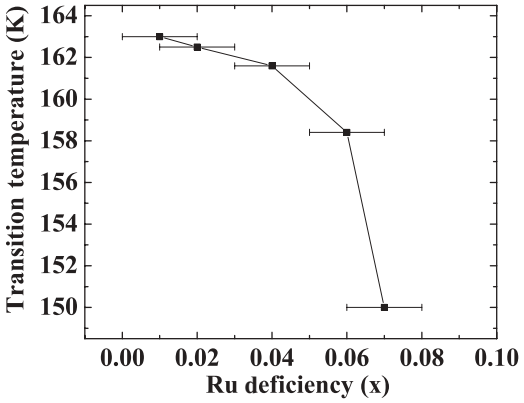

FIG. 12. Ferromagnetic transition temperature vs Ru-deficiency plot.

Furthermore, the peak height increases with the increase in the halting time. This observation conspicuously reflects its direct connection to the multivalley energy landscape picture as described earlier. As the system is halted for longer and longer times, it tries to uncover deeper and deeper valleys. Eventually, the response gets reflected in the $\Delta\chi'$ vs the T plot with an increase in the height of the peak, and this truly substantiates the multivalley picture in the context of glassy physics. In Fig. 13(b), we show the $\Delta\chi' = (\chi'_{\rm ref} - \chi'_{\rm halt})$ vs the T plot for $SrRu_{0.94\pm0.01}O_3$ at the same halting temperature of 40 K and with a halting duration of 8 h. Here, we also see a peak around the halting temperature, revealing the signature of the memory effect. In essence, all the samples, with compositions varying from 0.01 ± 0.01 to 0.07 ± 0.01, with respect to Ru deficiency, exhibit the characteristics of glassy behavior.

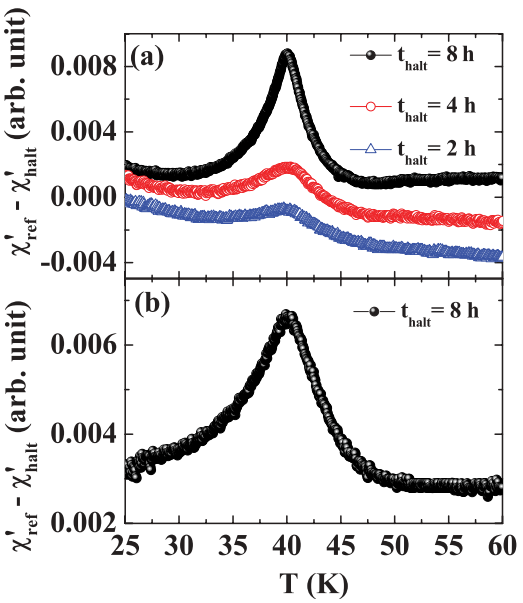

FIG. 13. (Color online) The differential in-phase ac susceptibility $\Delta\chi' = (\chi'_{\rm ref} - \chi'_{\rm halt})$ vs the T plot at a particular halting temperature of 40 K for (a) $SrRu_{0.99\pm0.01}O_3$ and (b) $SrRu_{0.94\pm0.01}O_3$.

Hence, we strongly believe that the stoichiometry in relation to Ru content cannot be accounted for by the observed glassy behavior in the $SrRuO_3$ system.

Based on the above findings, we firmly believe that the puzzling low-temperature magnetic and transport behaviors in $SrRuO_3$ can be linked to the change in lattice parameters that occur around the same temperature range. It is plausible that the structural modulation at low temperatures could be one of the possible reasons, which can induce the weak antiferromagnetic interaction that is responsible for nonsaturating magnetization and glassy behavior.

V. CONCLUSION

We performed structural, magnetic, and transport measurements to elucidate some of the most striking unusual physical responses of $SrRuO_3$. Two sets of polycrystalline $SrRuO_3$ samples with unique ordering temperatures were synthesized. Both samples were found to crystallize in an orthorhombic crystal structure with the *Pnma* space group. The low-temperature magnetization was found to be well described by the Bloch $T^{3/2}$ law, and the magnetization near T_c was found to follow the scaling law $M \sim (T_c - T)^{\beta}$ with $\beta = 0.35$ and $\beta = 0.30$ for SRO and SROD, respectively, signifying the 3D Ising behavior. The M-H plots exhibited a nonsaturating tendency uncovering the itinerant ferromagnetic behavior. The magnetic ac susceptibility study exhibited a broad hump far below the ferromagnetic ordering temperature, and the frequency dependence of this hump position exhibited the characteristic of multiple relaxations. Most strikingly, we noticed the low-temperature glassy magnetic behavior as clearly demonstrated by the time-dependent memory effect. This was very surprising and unlikely to happen in systems, which had itinerant ferromagnetic character. However, we conjectured that slow domain growth and spin canting could be the cause for such an effect. The transport study evidenced a crossover from FL to NFL behavior around 40 K and a slope change in the $d\rho/dT$ vs the T plot in the vicinity of that temperature. Astonishingly, we observed two distinct dips (one around the ferromagnetic ordering temperature and the other far below the ferromagnetic ordering temperature) in the temperature-dependent MR response. In addition, we observed the signature of an unusual dip in the temperature-dependent coercive field toward the low-temperature side. The emergence of such unusual magnetic and transport responses is strongly believed to be connected with a hidden magnetic interaction. Our effort on the neutron-diffraction study was able to trace the cause of such a hidden magnetic interaction. The findings of the neutron-diffraction study evidenced the change in the unit-cell lattice parameters around 75 K and that could be the central cause behind such anomalous low-temperature magnetic responses.

*Corresponding author: anil@physics.iisc.ernet.in

[1] R. J. Cava, Dalton Trans. 2979 (2004).
[2] P. Khalifah, R. Osborn, Q. Huang, H. W. Zandbergen, R. Jin, Y. Liu, D. Mandrus, and R. J. Cava, Science **297**, 2237 (2002).
[3] J. M. Longo, P. M. Raccah, and J. B. Goodenough, J. Appl. Phys. **39**, 1327 (1968).
[4] P. B. Allen, H. Berger, O. Chauvet, L. Forro, T. Jarlborg, A. Junod, B. Revaz, and G. Santi, Phys. Rev. B **53**, 4393 (1996).
[5] P. A. Joy, S. K. Date, and P. S. A. Kumar, Phys. Rev. B **56**, 2324 (1997).
[6] Y. Maeno, H. Hashimoto, K. Yoshida, S. Nishizaki, T. Fujita, J. G. Bendroz, and F. Lichtenberg, Nature (London) **372**, 532 (1996).
[7] A. P. Mackenzie and Y. Maeno, Rev. Mod. Phys. **75**, 657 (2003).
[8] S. N. Ruddlesden and P. Popper, Acta Crystallogr. **10**, 538 (1957).
[9] S. N. Ruddlesden and P. Popper, Acta Crystallogr. **11**, 54 (1958).
[10] R. Palai, H. Huhtinen, J. F. Scott, and R. S. Katiyar, Phys. Rev. B **79**, 104413 (2009).
[11] A. Kanbayasi, J. Phys. Soc. Jpn. **41**, 1876 (1976).
[12] A. Kanbayasi, J. Phys. Soc. Jpn. **41**, 1879 (1976).
[13] P. Kostic, Y. Okada, N. C. Collins, Z. Schlesinger, J. W. Reiner, L. Klein, A. Kapitulnik, T. H. Geballe, and M. R. Beasley, Phys. Rev. Lett. **81**, 2498 (1998).
[14] L. Klein, L. Antognazza, T. H. Geballe, M. R. Beasley, and A. Kapitulnik, Phys. Rev. B **60**, 1448 (1999).
[15] J. Okamoto, T. Mizokawa, A. Fujimori, I. Hase, M. Nohara, H. Takagi, Y. Takeda, and M. Takano, Phys. Rev. B **60**, 2281 (1998).
[16] J. S. Lee, Y. S. Lee, T. W. Noh, Y. Yoshida, S. I. Ikeda, J. Yu, and C. B. Eom, Phys. Rev. B **70**, 085103 (2004).
[17] I. I. Mazin and D. J. Singh, Phys. Rev. B **56**, 2556 (1997).
[18] J. M. Rondinelli, N. M. Caffrey, S. Sanvito, and N. A. Spaldin, Phys. Rev. B **78**, 155107 (2008).
[19] L. Klein, J. R. Reiner, T. H. Geballe, M. R. Beasley, and A. Kapitulnik, Phys. Rev. B **61**, R7842 (2000).
[20] T. Kiyama, K. Yoshimura, K. Kosuge, Y. Ikeda, and Y. Bando, Phys. Rev. B **54**, R756 (1996).
[21] M. S. Laad and E. Müller-Hartmann, Phys. Rev. Lett. **87**, 246402 (2001).
[22] L. Klein, J. S. Dodge, C. H. Ahn, G. J. Snyder, T. H. Geballe, M. R. Beasley, and A. Kapitulnik, Phys. Rev. Lett. **77**, 2774 (1996).
[23] M. S. Laad, I. Bradarić, and F. V. Kusmartsev, Phys. Rev. Lett. **100**, 096402 (2008).
[24] L. Klein, Y. Kats, A. F. Marshall, J. W. Reiner, T. H. Geballe, M. R. Beasley, and A. Kapitulnik, Phys. Rev. Lett. **84**, 6090 (2000).
[25] H. T. Jeng, S. H. Lin, and C. S. Hsue, Phys. Rev. Lett. **97**, 067002 (2006).
[26] W. Bensch, H. W. Schmalle, and A. Reller, Solid State Ionics **43**, 171 (1990).
[27] Y. Noro and S. Miyahara, J. Phys. Soc. Jpn. **27**, 518A (1969).
[28] C. W. Jones, P. D. Battle, P. Lightfoot, and W. T. A. Harrison, Acta Crystallogr., Sect. C: Cryst. Struct. Commun. **45**, 365 (1989).
[29] J. S. Dodge, C. P. Weber, J. Corson, J. Orenstein, Z. Schlesinger, J. W. Reiner, and M. R. Beasley, Phys. Rev. Lett. **85** 4932 (2000).
[30] Y. S. Lee, J. Yu, J. S. Lee, T. W. Noh, T.-H. Gimm, H.-Y. Choi, and C. B. Eom, Phys. Rev. B **66**, 041104(R) (2002).

[31] A. Koriyama, M. Ishizaki, T. C. Ozawa, T. Taniguchi, Y. Nagata, H. Samatab, Y. Kobayashi, and Y. Noro, J. Alloys Compd. **372**, 58 (2004).
[32] G. Cao, S. McCall, M. Shepard, J. E. Crow, and R. P. Guertin, Phys. Rev. B **56**, 321 (1997).
[33] G. Santi and T. Jarlborg, J. Phys.: Condens. Matter **9**, 9563 (1997).
[34] A. T. Zayak, X. Huang, J. B. Neaton, and K. M. Rabe, Phys. Rev. B **77**, 214410 (2008).
[35] S. Reich, Y. Tsabba, and G. Cao, J. Magn. Magn. Mater. **202**, 119 (1999).
[36] L. Pi, S. Zhang, S. Tan, and Y. Zhanga, Appl. Phys. Lett. **88**, 102502 (2006).
[37] P. Ravindran, P. Vajeeston, A. Kjekshus, H. Fjellvag, B. C. Hauback, Solid State Commun. **124**, 293 (2002).
[38] A. C. Larson and R. B. Von Dreele, GSAS Report No. LAUR 86-748, 1994 (unpublished); B. H. Toby, J. Appl. Crystallogr. **34**, 210 (2001).
[39] R. J. Bouchard and J. L. Gillson, Mater. Res. Bull. **7**, 873 (1972).
[40] S. Blundell, *Magnetism in Condensed Matter* (Oxford University Press, New York, 2001), p.119.
[41] Y. Kats, L. Klein, J. W. Reiner, T. H. Geballe, M. R. Beasley, and A. Kapitulnik, Phys. Rev. B **63**, 054435 (2001).
[42] D. Kim, B. L. Zink, F. Hellman, S. McCall, G. Cao, and J. E. Crow, Phys. Rev. B **67**, 100406(R) (2003).
[43] L. M. Wang, H. E. Horng, and H. C. Yang, Phys. Rev. B **70**, 014433 (2004).
[44] P. J. Baker, T. Lancaster, S. J. Blundell, M. L. Brooks, W. Hayes, D. Prabhakaran, and F. L. Pratt, Phys. Rev. B **72**, 104414 (2005).
[45] D. Samal and P. S. A. Kumar, J. Phys.: Condens. Matter **23**, 016001 (2011).
[46] K. Manna, D. Samal, S. Elizabeth, H. L. Bhat, and P. S. A. Kumar, J. Phys. Chem. C **115**, 13985 (2011).
[47] Y.-k. Tang, Y. Sun, and Z.-H. Cheng, Phys. Rev. B **73**, 012409 (2006).
[48] A. K. Kundu, P. Nordblad, and C. N. R. Rao, Phys. Rev. B **72**, 144423 (2005).
[49] E. Vincent, V. Dupuis, M. Alba, J. Hammann, and J. P. Bouchaud, Europhys. Lett. **50**, 674 (2000).
[50] S. Miyashita and E. Vincent, Eur. Phys. J. B **22**, 203 (2001).
[51] P. Mahadevan, F. Aryasetiawan, A. Janotti, and T. Sasaki, Phys. Rev. B **80**, 035106 (2009).
[52] L. Capogna, A. P. Mackenzie, R. S. Perry, S. A. Grigera, L. M. Galvin, P. Raychaudhuri, and A. J. Schofield, Phys. Rev. Lett. **88**, 076602 (2002).
[53] G. Herranz, V. Laukhin, F. Sánchez, P. Levy, C. Ferrater, M. V. García-Cuenca, M. Varela, and J. Fontcuberta, Phys. Rev. B **77**, 165114 (2008).
[54] L. Klein, J. S. Dodge, C. H. Ahn, J. W. Reiner, L. Mieville, T. H. Geballe, M. R. Beasley, and A. Kapitulnik, J. Phys.: Condens. Matter **8**, 10111 (1996).
[55] S. N. Bushmelevaa, V. Y. Pomjakushinb, E. V. Pomjakushinab, D. V. Sheptyakovb, A. M. Balagurova, J. Magn. Magn. Mater. **305**, 491 (2006).
[56] B. Dabrowski, O. Chmaissem, P. W. Klamut, S. Kolesnik, M. Maxwell, J. Mais, Y. Ito, B. D. Armstrong, J. D. Jorgensen, and S. Short, Phys. Rev. B **70**, 014423 (2004).